USING THE THERMAL WIND RELATIONSHIP TO IMPROVE OFFSHORE AND COASTAL FORECASTS OF EXTRATROPICAL CYCLONE SURFACE WINDS

James B. Truitt
NOAA/National Weather Service
Weather Forecast Office
Juneau, Alaska

Abstract

Land-falling oceanic cyclones in the midlatitudes confront the forecaster with a specific problem: they typically develop in data-sparse regions before they approach a coastal forecast area, making numerical model predictions more uncertain and the forecasting of surface winds more difficult. Errors in surface wind forecasts can deeply affect coastal mariners and communities. This article describes an alert system that helps the forecaster detect stronger synoptic-scale thermal gradients than otherwise expected and therefore identifies significant numerical forecast errors of cyclogenesis and associated surface wind.

A thermal-wind observation that is significantly stronger than the numerical model forecast value can indicate significant errors in the modeled cyclone evolution, typically including surface winds. The thermal wind observation is feasible in two steps: (1) an identification of regions suitable for the quasi-geostrophic assumption, and (2) a thermal-wind calculation that can be compared to the numerical model prediction of thermal wind. Our ability to discern when and where to apply the quasi-geostrophic assumption has significantly improved over the last 20 years, especially for the analysis of the thermal gradients associated with midlatitude oceanic cyclogenesis, and this progress is briefly reviewed. Synoptic-scale regions of quasi-geostrophic flow can typically be identified using satellite imagery, although other data are useful to confirm the absence of sources of strong ageostrophy such as deep convection and jet streaks. North Pacific extratropical cyclones moving toward the West Coast typically have a synoptic-scale region where the geostrophic approximation is valid; and it arrives onshore before the strong ageostrophies associated with upper level jet streaks. This sequence of events during landfall permits wind shear-based estimates of the thermal wind to be compared to the numerical model value before the cyclone can generate stronger than forecast surface winds in coastal regions. The thermal wind observation period has ended when the jet streaks are within subsynoptic range of the coastal wind profile site. Single significant-figure observations are sufficient to alert forecasters of possible errors in the numerical surface wind forecasts. An example is given using data from a rawinsonde and a Weather Surveillance Radar-1988 Doppler (WSR-88D) during a forecast shift at the National Weather Service Weather Forecast Office (WFO) in Juneau, Alaska. Based on the success of these results, suggestions for further research are provided.

Corresponding author address: James B. Truitt
4936 Hummingbird Lane
Juneau, Alaska 99801-9230
E-mail: james.truitt@noaa.gov

1. Introduction

The forecasting of mid-latitude oceanic cyclones is important to operational meteorologists in coastal regions. Such cyclones can develop in a data-sparse location shortly before moving into a coastal forecast domain, and major numerical model busts still occur (McMurdie and Mass 2004). In these cases, the forecaster needs to detect the largest departures from the model forecasts as early as possible.

Figure 1 indicates the locations of several forecast offices that routinely need to predict midlatitude oceanic cyclone evolution in the North Pacific Ocean. The cases detailed by McMurdie and Mass (2004) occurred near the southern boundary of the region shown in Fig. 1. Figure 1 also indicates the locations of all wind profile sites discussed below.

Observations near oceanic cyclones are sparse, although relatively more abundant at the surface and the jet level than the intermediate layer. Surface data include widely scattered ship and buoy reports, and occasional surface winds derived from satellite scatterometer measurements. The upper-level data include Geostationary Operational Environmental Satellite (GOES) visible and infrared imagery, cloud-track GOES winds, and observations from the Aeronautical Radio, Incorporated, Communication, Addressing and Reporting System (ACARS)(Benjamin et al. 1999).

Low observation densities are especially evident between the sea level and the cloud tops of oceanic cyclones. A variety of satellite imagery is available, but except for data from Microwave Sounding Units (MSU) (Kidder and Vonder Haar 1995), a cirrus shield can block the detection of lower-tropospheric features, and furthermore, this concealing cloud shield can track in phase with the wave for a long time. Rawinsondes and dropsondes (Douglas 1990) are typically unavailable, except during specially funded research projects. Note that this data density problem is typically not solved by ACARS, since these observations are irregular (Businger et al. 2001) and oceanic overflights typically use jet cruising levels for long distances.

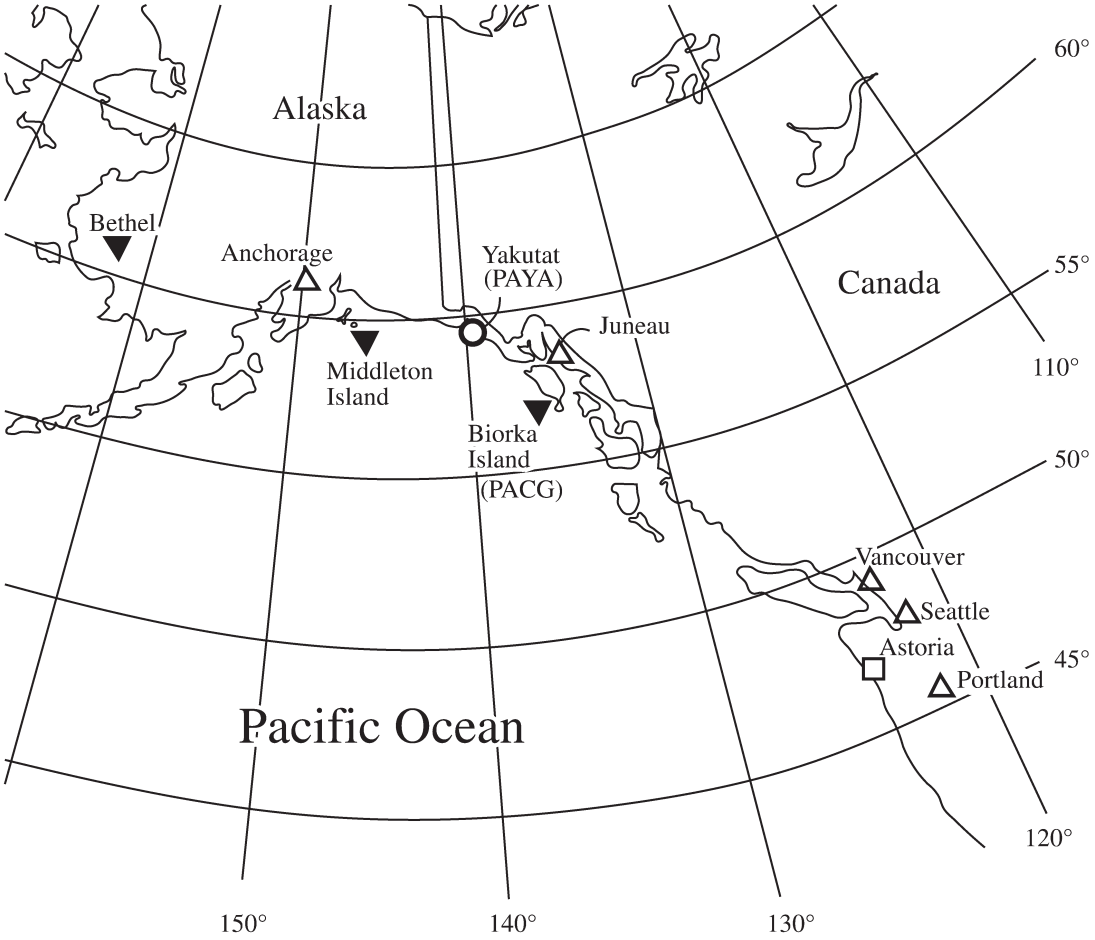

Fig. 1. Location of Yakutat rawinsonde site (circle), Doppler radar sites (dark triangles) shown for the outer coast and offshore islands, a temporary wind profile site (open square), and Forecast Offices (open triangles).

The operational meteorologist can monitor coastal vertical wind profiles in near real time from rawinsondes or WSR-88D radars, but it may be difficult at times to identify significant differences between the observed wind profile and the model values. Discrepancies in wind speed and speed shear can be readily seen, but important differences in directional shear can be difficult to detect visually (Koch 2001).

The thick layer of low data density can negatively impact the computer models' representation of a cyclone, and consequently limit the coastal forecaster's Situational Awareness (SA). The problem is that the thick layer contains unknown values for fields that are crucial to the correct forecasting of cyclone evolution such as

the baroclinicity. Forecasters in coastal regions sometimes have to wait for the cyclone to be onshore before learning how well the operational models performed. Large errors are sometimes observed.

The forecaster can learn much about a cyclogenetic system if a thermal wind observation (TWO) becomes available. For example, the baroclinicity can be conveniently estimated (Pettersen 1956). Also, as emphasized in this article, the thermal wind is a measure of the horizontal temperature gradient. Thermal wind values can be estimated by calculations using a vertical wind profile or a plan-view array of thickness values, provided the geostrophic component is significantly larger than the ageostrophic component. This condition is often called the geostrophic approximation.

This article describes a method to retrieve a TWO from the data-sparse layer associated with midlatitude oceanic cyclogenesis. If this TWO is stronger than a numerical model value for the corresponding location, then it is associated with stronger subsequent cyclogenesis and surface winds than the model forecast. These associations do not require measurement of surface pressure, and therefore the method can be applied to the analysis of oceanic cyclones in data-sparse regions.

Our ability to discern when and where to apply the quasi-geostrophic approximation has significantly improved over the last 60 years. Forsythe (1945) described how the approximation seemed valuable for calculating thermal wind values, but also mentioned that upper air analysts experienced unexplained failures. The quasi-geostrophic approximation has subsequently been deemed "generally useful" (Neiman and Shapiro 1989) with exceptions that fit into five categories: deep convection, strongly-curved geopotential height contours, pronounced orographic barriers, the boundary layer, and jet streak entrance and exit regions. Neiman and Shapiro (1989) and Koch (2001) have used the thermal wind equation to retrieve horizontal thermal gradients in cases involving upper tropospheric jet stream frontal zones. Neiman and Shapiro (1989) used single-station hourly profiler observations to estimate thermal gradients and their associated temperature advections in the vicinity of baroclinic zones. They elaborate on the seminal article by Forsythe (1945), and identify cases where quasigeostrophy should not be assumed. Koch (2001) used mesoscale models and products from the WSR-88D, including a thermal-wind method applied to the Vertical Wind Profile (VWP) data, to study a split front and the associated convective rainband in the southeastern United States. He compared the measurements to mesoscale model forecasts and evaluates the usefulness of the geostrophic assumption. His case study depicts a quasi-geostrophic part of a jet-front system reaching a WSR-88D site before the arrival of significant ageostrophic features closer to a jet stream.

Expanding on this thermal-wind approach using the VWP and rawinsonde data, an analysis technique for landfalling cyclones is presented here, where baroclinicity is estimated over thick layers from the troposphere above the boundary layer. These measurements are useful even if only accurate to within one significant figure because that is sufficient to alert the forecaster of possible large errors in the numerical forecasts. Section 2 briefly reviews the thermal wind equation and the conversion of potential energy to kinetic energy during cyclogenesis. Section 3 explains how a quasi-geostrophic region can be identified during midlatitude oceanic cyclogenesis based on the Neiman and Shapiro categories, along with analyses of scale. In Section 4, we apply the conceptual model to locations near these cyclones where the thermal wind method is especially useful. A case study is presented in Section 5 to illustrate the usefulness of the technique, followed by a frequency of use evaluation in Section 6. Section 7 is a discussion with suggestions for further research and Section 8 gives the conclusions.

2. Thermal Wind and Evaluation of Cyclogenesis

During the approach of oceanic cyclones, coastal wind profiles and satellite MSUs offer the possibility of retrieving model-independent thermal wind values. If the thermal wind is a valid indicator of cyclone intensity, the retrieved data can be compared to numerical model values of thermal wind and therefore indicate the accuracy of the model forecast of cyclogenesis, including the wind field.

The thermal wind is defined as the vector subtraction of a lower-level geostrophic wind from an upper-level geostrophic wind.

$$\mathbf{V}_T \equiv \mathbf{V}_g(p_u) - \mathbf{V}_g(p_l) \qquad (1)$$

where $\mathbf{V}_T$ is the thermal wind vector, $\mathbf{V}_g$ is the geostrophic wind, p_u and p_l are two pressure levels, and $p_u < p_l$. $\mathbf{V}_T$ can be estimated from wind profile and sounding data if a quasi-geostrophic approximation is made.

Using the definition of geostrophic wind, the thermal wind may also be expressed as:

$$\mathbf{V}_T = \frac{1}{f}\mathbf{k} \times \nabla(\Phi_u - \Phi_l) \qquad (2)$$

where Φ is the geopotential, f is the Coriolis parameter, and $\mathbf{k}$ is the unit vector along the z-axis (vertical).

Equation (2) can be used for calculating thermal-wind values from model thickness fields, $\Phi_u - \Phi_l$.

A schematic example of how these equations might be applied to a cyclogenetic system is shown in Fig. 2 (after Young and Grant 1995, Fig. 5.1.4a), where the magnitude of the thermal wind is proportional to the thickness gradient and the length of the arrow would increase (decrease) as the thickness gradient increases (decreases). This figure also illustrates that the thermal wind is parallel to thickness contours, with lower values (cold air) to the left of the vector, and that its strength is proportional to the magnitude of the thickness (thermal) gradient.

Figure 2 also contains a callout that graphically applies Eq. (1), and the outlined arrow is the same vector as that shown within the thickness field. Therefore Fig. 2 depicts how the shear of geostrophic winds can be used to calculate the horizontal temperature gradient. This gradient, and how it might change, has diagnostic value including that an increase in the horizontal temperature gradient provides additional potential energy to a perturbed state that is available for conversion to kinetic energy (Carlson 1991). This observation of thickness gradient can also be compared to the numerical model value by the forecaster.

Assume that we have a loop of satellite imagery that ends with a cloud pattern as depicted in Fig. 2 and that these images agree with numerical model fields for the cyclone's track and upper-tropospheric features, including the size and shape of the cloud shield. Further assume that GOES cloud-track winds and ACARS also corroborate the numerical model solution. We only have the numerical model data to depict the deep layer between the cirrus shield and the ocean surface. The problem is that the data ingested by the model has been limited since the cloud shield developed and began to travel in phase with the perturbation. We are depending on the model to simulate a variety of physical processes, including the conditions within the growing void of observational data. While not a closed system, the kinetic energy of a cyclone derives from the available potential energy released in the rearrangement of the air masses (Reed 1990), and the numerical model provides an approximation of this process along with the subsequent wind field.

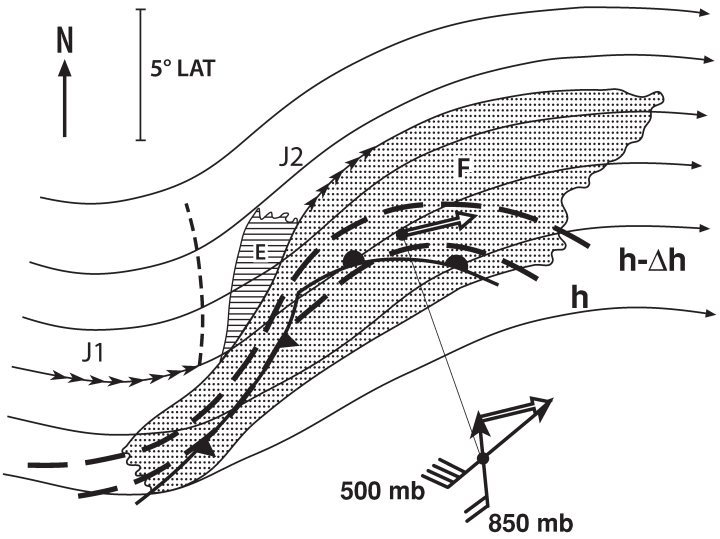

Fig. 2. Schematic showing a leaf cloud (stippling) during cyclogenesis (after Young and Grant 1995, Fig. 5.1.4a, p. 208) with additional conceptual model details (after Holton 1992, Fig. 6.5). Mid-level cloud E (hatching) has emerged from under cirrus shield F (stippling) between jet streaks J1 and J2 (arrow heads). Upper-level stream lines (long arrows) indicate flow through short-wave trough aloft (dashed line). Surface fronts (conventional notation) show an inflection point. Thickness between the streamlines is shown as heavy dashed lines, with a thermal wind vector (outlined arrow) consistent with the local thickness gradient at the vectors' base. Figure callout illustrates the relationship of the thermal wind (outlined arrow) to the geostrophic winds at 850 and 500 mb.

The model simulation of the processes in the hidden layer may become less representative of the real atmosphere, as time passes and the void of observational data persists through additional model runs. Therefore, observational data are still sought from the hidden layer.

If thermal-gradient observations then become available from underneath the cloud shield, they can show whether the potential energy available for cyclogenesis is significantly higher than the model depiction. If a significant amount of that higher potential energy is converted to kinetic energy in the cyclone, then the resulting surface winds should be consistent with having higher kinetic energy than the model. Based on forecaster experience, such changes typically include higher wind speeds in the lower troposphere and at the surface. Cases also occur that are similar to the depictions in McMurdie and Mass (2004) where the subsequent cyclone evolution is too different from the numerical model solution to be usefully compared.

The forecaster will prefer computer model(s) with a representative simulation of the potential energy available for that conversion. If the values retrieved from observations using Eq. (1) are significantly higher than the values predicted by the models using Eq. (2), the forecaster will subjectively strengthen the model solution. Such a comparison technique is useful even if the observational data are at a single location because the most important cyclone mechanisms are synoptic-scale processes (Parsons and Smith 2004).

The literature has long mentioned cases where Eq. (1) was applied to actual winds with a "lack of success" (Forsythe 1945). Such failures result from sources of error described by Neiman and Shapiro (1989). The largest sources of error would be from the presence of one or more

of the five categories of strong ageostrophy. Additional errors should result from the application of Eq. (1) in place of the complete thermal wind equation (Neiman and Shapiro 1989), but consistent with Forsythe (1945), such errors should be an order of magnitude smaller. Therefore the forecaster would benefit from a diagnostic method that checks the validity of the geostrophic approximation for the observed wind profiles.

3. Regions Containing Strong Ageostrophy

Considering thermal wind observations in real-time begins by first seeking to identify a sector within the oceanic cyclone that has the associated baroclinicity, yet where the actual winds have a geostrophic component significantly larger than the ageostrophic component. This section shows that the strong ageostrophies near such cyclones are sufficiently limited in spatial scale, such that an adjacent sector suitable for the geostrophic assumption and contributing to cyclogenesis can be identified.

a. Synoptic-scale regions containing strong ageostrophy

The Neiman and Shapiro (1989) exceptions to the validity of the quasi-geostrophic assumption can be identified using data and techniques already available to operational meteorologists: (1) Deep convection can be detected using satellite imagery or WSR-88D reflectivity data. (2) Strongly curved geopotential height contours, along with other sources of error such as data corruption due to velocity aliasing, should be detectable using WSR-88D velocity data displayed with the VWP root mean squared error (RMSE). (3) Pronounced orographic barriers on the outer coast can produce barrier jets that are not significant above the terrain level (Parish 1982). (4) Boundary layer effects over oceans and shallow coastal terrain can typically be neglected by not using data below the 850-mb level; however, a method for forecasting surface wind must still account for a transition through the boundary layer.

The remaining exception to the validity of the quasi-geostrophic approximation (Neiman and Shapiro 1989) is from upper-level jet streaks. The location of a jet stream and the existence of jet streak entrance and exit regions are easily identified using satellite imagery (Kidder and Vonder Haar 1995). Note that the jet stream is intrinsic to cyclone evolution (Reed 1990) and therefore routinely exists within synoptic-scale distances of the cyclogenetic baroclinicity field one seeks to sample. Consequently, the topic of the strong ageostrophy associated with jet streaks is emphasized in this article. We will now use an existing conceptual model of cyclone development to identify a sector where the geostrophic approximation is useful.

b. Scale of strong jet streak ageostrophies

A useful measure of the validity of the geostrophic approximation is the Rossby number (R_0), which is defined as the ratio of the characteristic scales of ageostrophic acceleration to the Coriolis acceleration:

$$R_0 \equiv \frac{U}{fL} \qquad (3)$$

where U is the velocity scale, f is the Coriolis parameter, and L is the horizontal length scale. The Rossby number is typically of order 0.1 for midlatitude synoptic-scale systems (Holton 1992) and of order 1.0 in the presence of jet streaks on subsynoptic scales (Bluestein 1993).

When $R_0 \sim 0.1$, the quasi-geostrophic approximation can be made, although the thermal wind calculation is limited to one significant figure accuracy. A comparison of the results of Eq. (1) using wind observations, with Eq. (2) using model thickness fields, can reveal large errors in the model estimate of available energy.

Actual measurement of R_0 is not practical; however, numerical model fields of R_0 were temporarily available at WFO Juneau, and were applied to the thermal wind method. Cases of $R_0=0.2$ occurred, along with one case of $R_0=0.3$. These cases have been used to estimate a threshold value for the significance of the ratio of observed thermal wind magnitude over model thermal wind magnitude. If the ratio is above 1.3, then the measured thermal wind value is significantly higher than the model value, with increasing values having increasing significance.

In subsynoptic regions where $R_0 \sim 1$, Eq. (1) is inapplicable and therefore cannot be used to identify errors in the model estimate of available energy. Furthermore, the vertical coupling of ageostrophic winds associated with isotach maxima can result in the depth of strong ageostrophy extending below the jet-stream level (Bluestein 1993). Therefore, Eq. (1) should not be applied to wind profile data from beneath the jet streaks. These ageostrophies are contained within a subset of the cyclogenetic region one seeks to sample for thermal gradients and the geostrophic approximation can be applied to the remainder of the region, as described below with a conceptual model.

4. Conceptual Model and Application

a. Cyclogenetic regions: quasigeostrophy vs. ageostrophy

An oceanic cyclogenetic system is depicted schematically in Fig. 2. The cirrus shield, depicted with the stippled area F, is commonly identified with infrared and water vapor imagery. Individual jet streaks along the

jet stream can be located using loops of such images, but the precision of streak identification is better transverse of the flow than along it. The details of the transverse/vertical circulations associated with jet streaks are beyond the scope of this article. $R_0 \sim 1$ should be occurring in the presence of these jet streaks on subsynoptic scales (Bluestein 1993). Similar strong ageostrophies are assumed near where the cirrus shield area F is depicted as adjacent cloud shield E, but will be harder to identify due to the complexity of the jet streaks that should soon couple. The horizontal extent of the strong ageostrophies is not known to a subsynoptic-scale resolution, i.e. we cannot correctly draw R_0 isopleths for various levels on Fig. 2. However, the jet streaks have locations relative to the cyclogenetic system that are routinely identified to subsynoptic scale precision by forecasters using satellite imagery. Such features exist on a smaller scale than the whole cyclone, and this is consistent with model studies that show the ageostrophic circulations associated with cyclones are typically an order of magnitude smaller than the geostrophic circulations (Anthes 1990). Let us assume the modeled cyclones accurately represent actual cyclones. In Fig. 2 the smaller scale region of ageostrophic circulations would include the jet streaks that the forecaster identifies in the western part of the cyclone.

Because the geostrophic circulations take place on a much larger scale, the thermal wind equations can be applied usefully. Assume that that the cyclone in Fig. 2 is in the North Pacific and is approaching a West Coast WSR-88D or wind profiler. Such a location under the cirrus shield is useful because of: (1) the obscuration by the cirrus shield, (2) the role of the thickness field in cyclone evolution, and (3) the jet streaks are still a synoptic scale distance offshore from the wind profile sites.

The flow becomes more ageostrophic as the jet streaks move within subsynoptic-scale range of the wind profile site, and the forecaster can anticipate this by using GOES satellite imagery or cloud motion winds to track the jet steaks synoptically. Therefore, when the jet streaks are within subsynoptic range of the data site the TWO period has ended. A tabular history of the TWOs is useful. For example, data from the WSR-88D site PACG (Biorka Island) (Fig. 1) is recorded along with the application of Eq. (1) by a computer script at WFO Juneau. The forecaster can then review a prior period of wind data collected sufficiently far ahead of these west coast land-falling strong ageostrophies that the quasi-geostrophic approximation is valid.

b. Forecasting oceanic cyclogenesis and surface wind

A diagnosis of cyclogenesis can be made by blending satellite data, conceptual models, numerical model solutions, and observations including thermal wind. The forecaster blends experience with a conceptual model of cyclogenesis that includes the conversion of potential energy to kinetic energy (Bluestein 1993). Usually, the thermal wind estimate calculated from wind profiles with Eq. (1) agrees to one significant figure with the corresponding numerical model solutions calculated with Eq. (2), which shows that the numerical forecast represents the energy conversion about to occur. However, a stronger thermal wind is associated with stronger cyclogenesis than the numerical model solution, and stronger cyclogenesis is associated with stronger surface wind. In such a case, the forecaster must adapt his or her analysis, as illustrated in the following example.

5. Forecast Shift Case Study

This case study from 11 January 2002 at WFO Juneau illustrates how the forecasting of winds associated with an oceanic cyclone during coastal approach can be improved with a baroclinicity calculation that provides an alert. TWOs were calculated with the PAYA (Yakutat) rawinsonde and the PACG WSR-88D wind profiles. The WSR-88D site was temporarily out of service when a measure of baroclinicity was first needed. The PAYA rawinsonde was first used by the forecasters for the wind-shear calculation and comparison with model data. The forecasters issued amendments based on these data, and then began to receive WSR-88D VWP data, which they used for updated evaluations. The wind speed units used in this section for the public forecasts and verification are mph ($m\ s^{-1}$), while kt ($m\ s^{-1}$) were employed for the marine forecasts and verification.. Table 1 shows the chronology of events that occurred during the forecast shift.

a. Real-time vs. hindsight calculations

Two thermal wind comparisons are provided in each case. First is an initial crude comparison used in real-time during the forecast shift; secondly a more stringent comparison is applied later in hindsight.

During the forecast shift, the magnitude of the thermal wind calculated with Eq. (1) from the 850-500 mb PAYA and PACG winds were compared with the magnitude of the thermal wind calculated with Eq. (2) from the 1000-500 mb layer Aviation (AVN) data. The 5000 ft (1524 m) PACG measurements were the lowest available winds due to the boundary layer constraint. Hindsight calculations using the AVN 850-500 mb layer are provided.

b. Forecast shift briefing

A GOES IR animation ending with the image at 0000 UTC 11 January 2002 (Fig. 3) indicated cyclogenesis and a northward track. The 0000 UTC National Center for Environmental Prediction (NCEP) surface map (Fig. 4) showed a surface low at 53° N, 143° W. The differences among the models were small, but the model of choice by the prior shift was the 1800 UTC 10 January 2002 run of the AVN Global Model and had therefore guided the forecast package issued to users. Output from this model run at 6 h, 12 h, and 18 h is shown in Figs. 5-7. Figure 5 shows AVN thermal wind values available closest to PAYA and PACG, as well as the corresponding model thickness field at 6 h. Figure 6 shows the same model features, with the addition of the surface pressure field and the low that is tracking north at 12 h. Figure 7 shows the same model features as Fig. 6, except for the thermal wind values are omitted as they are no longer used for comparison, at 18 h. Forecasters believed that the satellite imagery showed upper-tropospheric cyclogenesis with weak development in the lower troposphere, but the view was blocked by the extensive cloud shield (Fig. 3). Another problem was that the PACG WSR-88D site was out of service until 0308 UTC. The 0000 UTC PAYA rawinsonde was available but needed evaluation for usability with the geostrophic assumption. Therefore, the validity of the geostrophic assumption first needed to be established.

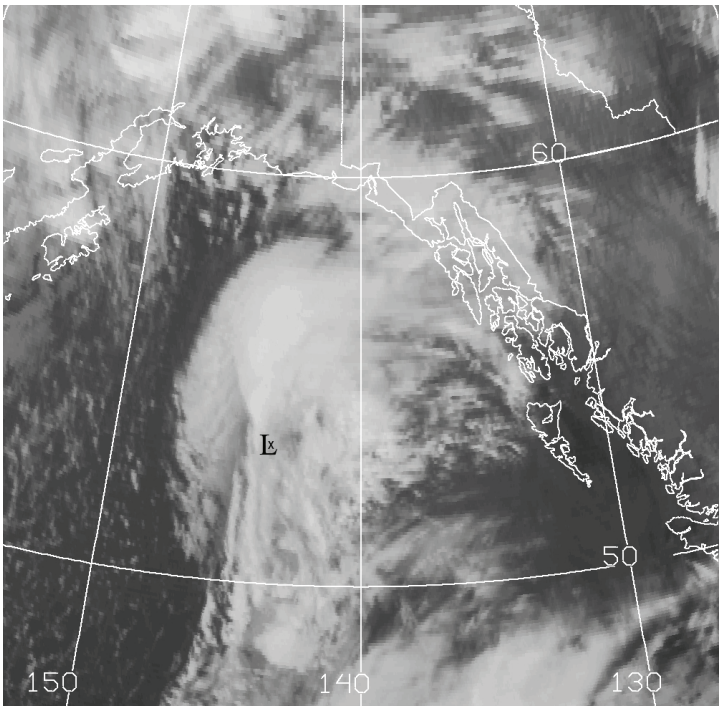

Fig. 3. Infrared GOES image for 0000 UTC, 11 January 2002. Capital L denotes approximate location of sea-level pressure minimum.

Time (UTC)	*Event*
1800	Last AVN model run on 10 January 2002
0000	Rawinsondes are completed, Fig. 4. map time
0020	Marine forecast issued
0030	Zone forecast issued, including Yakutat
0100	Forecasting crew change and notes started
~0145	PAYA rawinsonde data are used for calculation of thermal wind, Eq. (1)
0206	Marine forecast is amended
0211	Wind Advisory issued for Yakutat zone
0308	PACG data begins to arrive, including VWP
0313	PACG VWP data are used for calculation of thermal wind, Eq. (1)
~0330	PACG WSR-88D data diagnosed a validation of the amendments
0600	AVN model verification time (Fig. 6b)
0943	PAYA first 45 mph (20 m s^{-1}) gust
1200	Ship WCZ6534 verifies Gale
1242	PAYA gust of 46 mph (21 m s^{-1})

Table 1. Chronology of forecast shift 11 January 2002

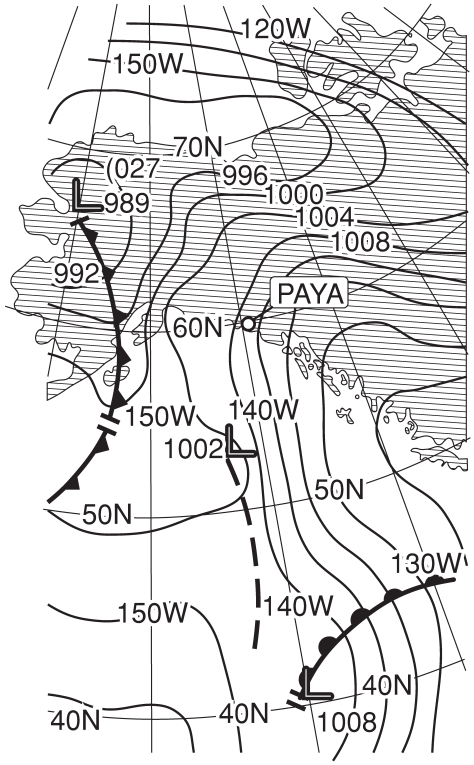

Fig. 4. 0000 UTC, 11 January 2002 NCEP surface analysis. Solid contours are isobars (mb). Dashed line indicates the pressure trough, and capital L's denote approximate locations of sea-level pressure minima. Standard symbols denote frontal boundaries. PAYA rawinsonde site is shown as open circle.

c. Applicability of the geostrophic approximation

The satellite imagery showed a baroclinic comma cloud with an upper-level inflection point in the vicinity of 54° N, 145° W (Fig. 3). Jet stream signatures extended upstream to the south, but not downstream toward the coast including PAYA and PACG. Based on the conceptual model of jet streaks with ongoing cyclogenesis, we assumed that the flow over the coastal region and adjacent ocean was quasi-geostrophic. The satellite imagery at 0000 UTC did not show convection along the outer coast to the NNE through E of the cyclone. Based on the conceptual model, the satellite imagery, and experience using the PAYA data (Truitt 1994), we decided that the baroclinicity could be calculated using the PAYA wind shears and Eq. (1).

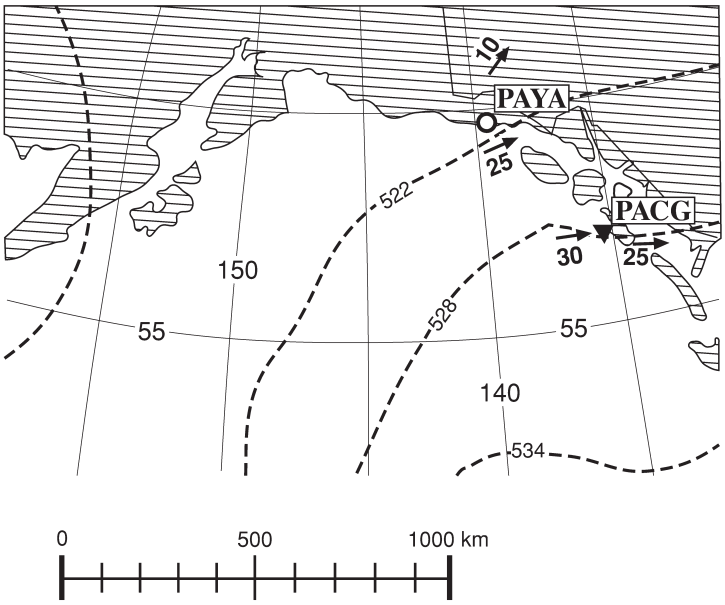

Fig. 5. AVN 6-h forecast of 1000-500 mb thickness contours (dashed, dam) and thermal wind vectors (kt), valid at 0000 UTC 11 January 2002. Locations of PAYA rawinsonde site (open circle) and PACG WSR-88D (dark triangle) are included.

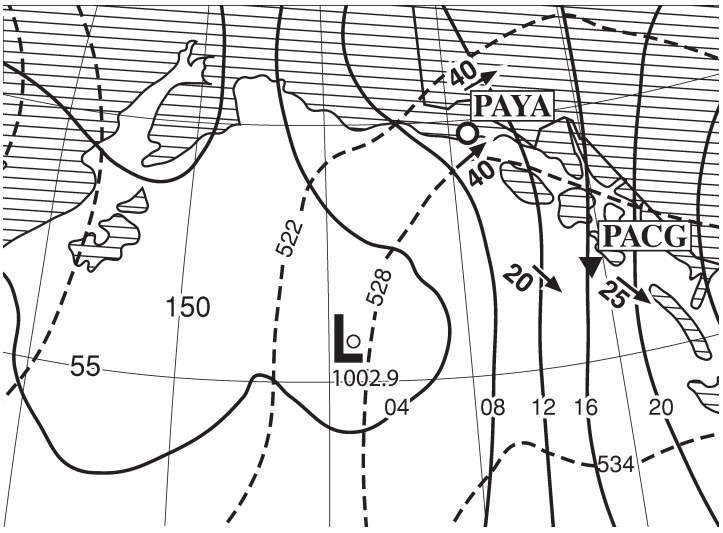

Fig. 6. AVN 12-h forecast of sea-level pressure (solid, mb), 1000-500 mb thickness contours (dashed, dam), and 850-500 mb thermal wind vectors (kt), valid at 0600 UTC 11 January 2002. Capital L indicates location of model sea-level pressure minimum. Locations of PAYA rawinsonde site (open circle) and PACG WSR-88D (dark triangle) are included.

The PACG WSR-88D became available with the 0308 UTC volume scan (Fig. 8). Based on the AVN cyclone track (Figs. 6 and 7), the forecaster assumed that jet streak ageostrophies would not reach the outer coast until many hours later.

The RMSE values for the winds in Fig. 8 (not shown) were less than 4 kt, which is consistent with a near-homogeneous wind field at all levels. We therefore assumed the PACG data shown in Fig. 8 to be quasi-geostrophic.

d. PAYA rawinsonde

The 0000 UTC PAYA rawinsonde 850-500-mb layer thermal wind was compared to the corresponding model solution to establish whether cyclogenesis should generally follow the AVN prediction. The PAYA thermal wind using Eq. (1) was 52 kt (27 m s^{-1}). The AVN thermal-wind magnitude retrieved with Eq. (2) was 25 kt (13 m s^{-1}) and this value is overlaid on Fig. 5. The magnitude of the thermal wind at PAYA was therefore roughly double what the model predicted.

As of 0000 UTC, the PACG WSR-88D was not yet reporting. The forecaster used three factors to subjectively estimate that the thermal wind near PACG was about half again what the model guidance showed: (1) The PAYA thermal wind observation had usefulness for a wide area including PACG, but diminishing with distance. (2) Accordingly, the numerical model thermal wind values needed to be factored in more for increasing distances from the PAYA data site. (3) The satellite imagery was used to estimate the size of the cyclogenetic system.

e. PACG WSR-88D VWP

The VWP from PACG (Fig. 8) first became available just after 0300 UTC, 11 January 2002. This was between the times of the AVN 6 and 12 hour forecasts valid at 0000 UTC and 0600 UTC 11 January 2002. Therefore, the magnitude of the thermal wind calculated with Eq. (1) was compared with the mean value of the AVN thermal wind magnitudes. We used the VAD (Velocity Azimuth Display) wind at 5,000 ft (1524 m) as an approximation for the 850 mb wind, and the VAD wind at 18,000 ft (5486 m) as an approximation for the 500-mb wind in Eq. (1).

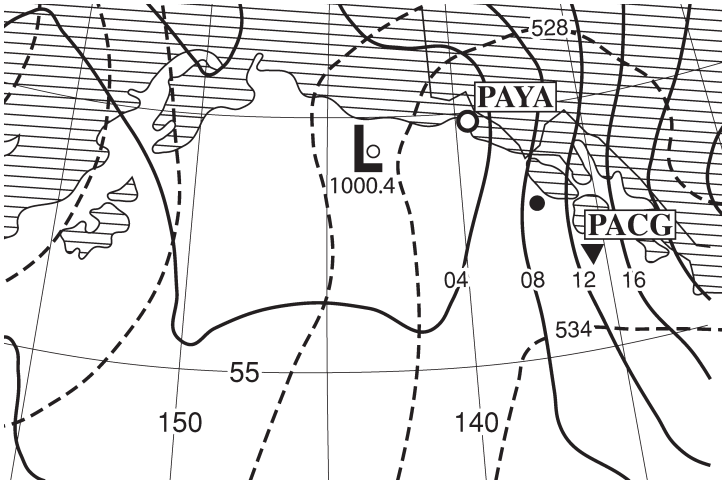

Fig. 7. As in Fig. 6, except 18-h forecast valid at 1200 UTC 11 January 2002. Note the inclusion of the location of the ship report from WCZ6534 (large black dot).

Based on these winds observed at 0313 UTC, the thermal wind at PACG was found to be 39 kt (20 m s^{-1}), while the AVN thermal-wind magnitude for PACG was 25 kt (13 m s^{-1}). This corresponds to a ratio of 1.5 between the measured value and the model value. Based on forecaster experience, the stronger cyclogenesis would result in peak surface winds near PACG nearly 50% stronger than those predicted by the AVN.

f. Amendments issued and verification received

The Yakutat Public Zone from 0020 UTC 11 January 2002 stated "winds becoming southeast to 25 mph (11 m s^{-1}) by the morning (of 11 January)." At 0211 UTC, a Wind Advisory was issued for the Yakutat Zone and the text was amended to "Southeast winds increasing with gusts to 50 mph (22 m s^{-1})" for the overnight period. At 0943 UTC, the winds at PAYA became southeast and increased to 24 mph (11 m s^{-1}). From 0953 UTC to 1153 UTC four peak wind values of 45 mph (20 m s^{-1}) occurred, and the highest wind of 46 mph (21 m s^{-1}) occurred at 1242 UTC and 1253 UTC.

Marine forecasts received corresponding amendments at 0206 UTC. Only one marine observation was to become available in the eastern Gulf of Alaska through 1200 UTC (Fig. 7) and the marine wind amendment for this location was based on a more conjectural use of the 0000 UTC PAYA TWO. The subsequent PACG TWO caused the forecasters to become more confident that the previously transmitted 0206 UTC marine amendment was appropriate for the eastern Gulf of Alaska closer to PACG. The original marine forecast for this location, issued at 0020 UTC, read "southeast winds less than 20 kt (10 m s^{-1}) increasing to southeast 25 kt (13 m s^{-1}) Thursday evening," with Thursday evening defined as 0300 UTC to 0900 UTC 11 January 2002. The forecast had no other wind increase overnight. The marine amendment transmitted at 0206 UTC read "southeast winds increasing to 40 kt (21 m s^{-1}) Thursday evening." At 1200 UTC 11 January 2002, ship *WCZ6534* reported winds southeast at 40 kt (21 m s^{-1}) (Fig. 7). In both cases, the TWO had improved the surface wind forecast.

g. Hindsight computations

The case study above described the calculations made during a forecast shift: a comparison of thermal wind values retrieved from 850-500-mb observed winds with the thermal wind values calculated from the AVN 1000-500-mb thickness. In hindsight, a comparison of thermal wind values retrieved from 850-500-mb PAYA winds (52 kt, or 27 m s^{-1}) with the thermal wind values calculated from the AVN 850-500-mb thickness (19 kt, or 10 m s^{-1}) yields a ratio of 2.7. A comparison of thermal wind values retrieved from 850-500-mb PACG winds (39 kt, or 20 m s^{-1}) with corresponding AVN 850-500-mb thermal wind (19 kt, or 10 m s^{-1}) yields a ratio of 2.0.

Note that using the AVN 850 mb level instead of 1000

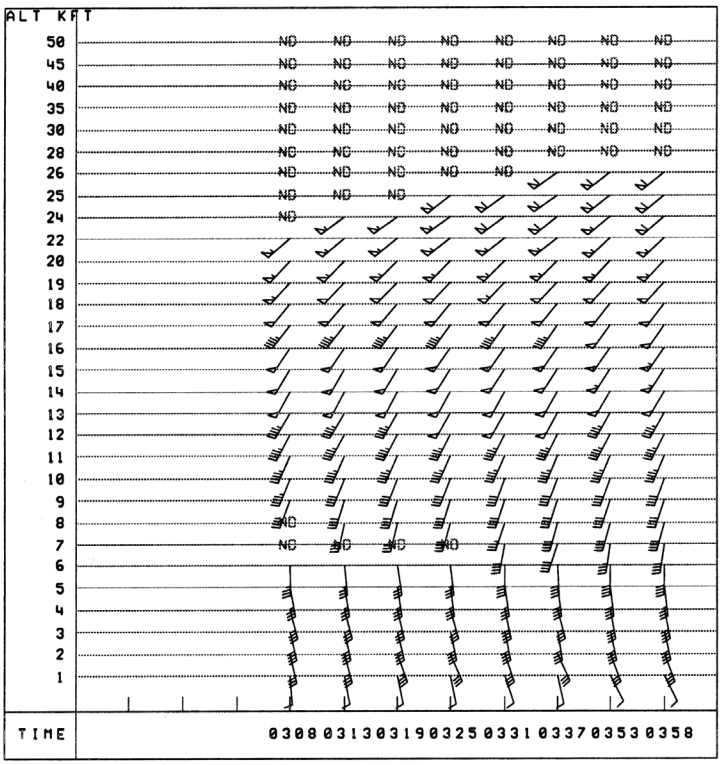

Fig. 8. VWP from PACG for 0308-0358 UTC 11 January 2002, as displayed on the Advanced Weather Interactive Processing System (AWIPS) at the NWS Juneau WFO. Standard wind barbs are shown in height scale for each 1000 ft (305 m). Second column of wind barbs depicts VWP ending at 0313 UTC used for shear calculation. The veering of wind is evident for a large depth.

mb reduced the thermal wind from 25 kt (13 m s^{-1}) to 19 kt (10 m s^{-1}), which increased the ratio to 2.7. The results validate the baroclinicity alert issued during the shift.

6. Rates of Occurrence

Case studies were logged during an early period (cool season of 1999-2000) in the techniques development. During this period, the forecasts used the TWOs as a predictor of surface winds for any cases where landfalling features such as cold fronts might result in a significant wind event. These cases are identified and included for the purpose of completeness. This broad application of the thermal wind method was based on a statistical study (Truitt 1994). The case studies typically did not differentiate between the marine forecasts and the forecasts for communities near sea level. The cases were classified into the following groups:

1) The TWO values were significantly higher than the numerical models (similar to the above case study). The surface winds were forecast and verified as significantly stronger than numerical model predictions (two cases).

2) The numerical model solutions had significantly different wind forecasts. The thermal wind method was used to choose the model with stronger winds and did verify, including a High Wind Warning (one case).

3) The thermal wind agreed with numerical model values and the documentation then ended (nine cases). In two of the cases there is indication that the forecaster did not expect cyclogenesis, but this detail is difficult to reconstruct.

4) The thermal wind was weaker than any model solutions and explosive cyclogenesis occurred as verified with ship data. The forecasters successfully applied the model solutions presumably using satellite imagery and other standard tools. The method failed (one case).

5) The thermal wind method was applied during obvious convection after a log entry of 'could these cells be severe.' The models depicted cyclogenesis and forecast winds were raised higher than numerical model solutions. The verification of the resulting wind advisory was claimed based on one gust but the log has ambiguity. The method should not have been applied (one case).

6) No cyclone, based on the available hardcopies of model analysis and GOES IR. A cold front was approaching at the time of application of the thermal wind method. The ratio of thermal wind over model values was 1.33. No documentation was found that indicated whether the forecasts differed from model depictions, or whether verification became available. The method should not have been applied (one case).

The number of cases here is too small for formal statistical analysis, but subjective comparisons with the subsequent seven years are practical. The first three categories have typical relative frequencies of occurrence. Failures have subsequently occurred but not for the reasons given in 4, 5 and 6. The subsequent failures have occurred when winds, stronger than depicted by the numerical models, occurred at high elevations in the interior mountains.

Failures such as (4) should sometimes still occur. The thermal wind method only samples the 850-500 mb layer, and does not identify upper tropospheric features. Skill is not claimed for cases where the TWO is weaker than the numerical model values, and they may result from layers with stronger thermal wind values either above or below the 850-500 mb sample layer. In (4) above, the forecasters used the model guidance and standard techniques successfully.

Cases where TWOs are stronger than the model values can have actual cyclone evolutions that differ from the model solutions in a variety of ways. The stronger surface winds can occur in locations that seem inexplicable using the model solutions. Such cases are hard to classify, but are roughly similar to McMurdie and Mass (2004).

7. Discussion and Proposed Future Research

In this study the data-sparse layer associated with a midlatitude oceanic cyclone was sampled for a thermal wind calculation, from which the forecasters had inferred that the cyclogenesis was to become stronger than predicted by operational computer models. The forecasts were updated, and the updates monitored, with the expectation that an increase in wind speeds would reach the surface.

This simple method should help provide direction to the research and numerical modeling communities. What the operational community needs most is for the numerical model performance to improve enough for such methods to be obsolete. Therefore, suggestions to the research community are provided, including some for future theoretical work.

For example, the numerical modeling community could research the creation of model ensembles that emphasize a range of thermal wind values and their subsequent cyclone evolutions. The theory of extratropical cyclones (Hoskins 1990) extends far beyond the method presented in this article, albeit the method is convenient for field operations.

Based on the literature (Carlson 1991; Reed 1990) we can typically expect stronger winds, or a significantly altered cyclone evolution when there is stronger thermal wind in the cyclogenetic region. The TWO and comparison tool is designed to calculate thermal wind from observations and compare it with the numerical model solution. Tests at the WFO Juneau demonstrate experimentally that we can improve our forecasts with this tool. Consequently, the reasoning was right and future work should investigate the mechanisms behind the relationship, as well as the reasons for the observed thermal wind values being stronger than the numerical model solution.

The TWO and comparison tool uses several simplifying assumptions but introduces error, especially when the observed values are stronger than the model values: (1) The existing numerical model results are typically applied with the assumption that the cyclone evolution will have little change except for the subjectively determined increases in wind speeds in the lower troposphere and the surface. (2) The increased thickness gradient may have several unknown causes. However, they are unknown and the result is the assumption that no differentiation exists that may affect cyclone evolution. (3) The complete thermal wind equation is not used, and most of the additional terms should be practical to implement (Neiman and Shapiro 1989). (4) The tool does not account for boundary layer complexities. These include friction, stratification, baroclinicity, turbulence, along with their interactions. In addition, the sensible and latent heat fluxes in the boundary layer can "fuel" the rapid development of oceanic extratropical systems (Uccellini 1990).

The data used for Eq. (1) need to come from above the boundary layer, yet the associated method must account for processes that transport momentum downward through the boundary layer to the surface. In addition, the coastal wind profile sites are typically located where the surface roughness changes from water to land and a deeper boundary layer. For example, experience in operational meteorology indicates the boundary layer over the ocean is below 3000 ft (914 m). However, tests using the PACG WSR-88D VWP show higher RMSE and obvious exceptions to homogeneous flow through 4000 ft (1219 m). An altitude of 5000 ft (1524 m) is assumed to be above the boundary for the purposes of the thermal wind tool, yet weak orographic influences have probably been detected at PACG even during onshore flow.

The case studies from 1999-2000 did not show method failures that have been observed in the following seven years. These subsequent failures have occurred when winds stronger than depicted by the numerical models were forecast, but the only winds significantly stronger than the models occurred at high elevations as reported by anemometers in the interior mountains near Juneau. In such cases the method seems to predict an increase in a cyclone's winds aloft that do not extend downward through the boundary layer until reaching topography above about 4000 ft (1219 m).

Cases where the TWO is weaker than the numerical model values cannot be usefully applied. It is possible that a strong baroclinic layer extends below 5000 ft (1524 m) that the numerical model depicts as being within the 850-500 mb layer. If this is so, it is also possible for the tool to fail to detect cases where the numerical model surface winds will not be strong enough.

The persistent void of observational data offshore may require soundings for significant improvement of numerical model performance. Dropsondes (Douglas 1990) could be placed offshore according to the conceptual model and synchronized for numerical model runs. The TWOs could also be calculated using winds at lower levels than is practical at sites like PACG, due to the shallower boundary layer over the ocean. Rapid changes are occurring in the field of Unpiloted Aircraft Systems (UAS) that should lower the cost per sounding. Satellite MSUs can also retrieve data through clouds (Kidder and Vonder Haar 1995). A comparison would be made between two applications of Eq. (2): the first using model thickness fields, the second using a field of thickness values from the MSU soundings. This second application of Eq. (2) would use finite-differencing to obtain the field of Φ_u-Φ_l for locations according to the conceptual model.

While the conceptual model presented above has broad operational applicability, the following limitations should be noted: (1) The complex terrain of western North America often generates strong ageostrophies at the data site if the cyclone is making landfall to the south, or if the cyclone is following a coastal track from the south. (2) The exact location of the jet streaks and associated ageostrophy can be difficult to determine. Cases have been observed at WFO Juneau when the wind began to back with height earlier than expected and are believed to be associated with ageostrophic frontal transverse circulations as described by Koch (2001). This early arrival of ageostrophies may be associated with mature occlusions as defined in the Norwegian conceptual model

of cyclone evolution. (3) Measurements at a data site can correspond to a preceding baroclinic wave. (4) The thermal wind for the 850-500-mb layer should also be calculated in two or more layers, such as 850-700 mb and 700-500 mb, to help identify cases where the strong thermal wind and baroclinicity could be limited to the upper layer, without extension to the boundary layer.

8. Conclusion

Historically, meteorologists have thought of the thermal wind as an elegant instruction tool, but much less as a useful analysis tool. The geostrophic approximation has a long history of failures (Forsythe 1945; Doswell 1991), and strong ageostrophies are significant features of extratropical cyclones. However, the identification of such ageostrophies has become more practical (Neiman and Shapiro 1989) and allows the identification of a synoptic-scale region within the cyclogenetic system suitable for the quasi-geostrophic approximation. The region suitable for assuming quasigeostrophy includes a low data-density volume under the cloud shield that travels in phase with the cyclogenetic wave.

The TWO is compared to the numerical model value. If the observation is significantly stronger than the model value, then at least one of three model-relative outcomes will occur: (1) raised wind speeds in the lower troposphere, (2) higher surface wind speeds, and (3) subsequent cyclone evolution too different from the model for operationally useful comparison.

For operational meteorologists, the thermal wind method can alert the forecasters of significant numerical model forecast errors. That such a simple approach can predict numerical model errors should help provide direction to the research community. For the research community, the thermal wind method described, emphasizes the need for sounding data (from satellites microwave sensors or aircraft) within oceanic midlatitude cyclogenetic systems.

Author

Jim Truitt is a Lead Forecaster at NOAA/National Weather Service Forecast Office in Juneau. He earned a B.S. in Meteorology from Texas A & M University. His long-term goals include improving the wind forecasting of extratropical cyclones in the North Pacific.

References

Anthes, R. A., 1990: Advances in the understanding and prediction of cyclone development with limited-area fine-mesh models. *Extratropical Cyclones: The Erik Palmén Memorial Volume,* C. W. Newton and E. O. Holopainen, Eds., Amer. Meteor. Soc., 221-253.

Benjamin, S. G., B. E. Schwartz, R. E. Cole, 1999: Accuracy of ACARS wind and temperature observations determined by collocation. *Wea. Forecasting*, 14, 1032-1038.

Bluestein, H. B., 1993: *Observations and Theory of Weather Systems. Vol 2, Synoptic-Dynamic Meteorology in the Midlatitudes,* Oxford University Press, 594 pp.

Businger, S., M. E. Adams, S. E. Koch, and M. L. Kaplan, 2001: Extraction of geopotential height and temperature structure from profiler and rawinsonde winds. *Mon. Wea. Rev.*, 129, 1729-1739.

Carlson, T. N., 1991: *Mid-Latitude Weather Systems.* HarperCollins Academic, 507 pp.

Doswell, C. A., III, 1991: A review for forecasters on the application of hodographs to forecasting severe thunderstorms. *Natl. Wea. Dig*., 16(1), 2-16.

Douglas, M. W., 1990: The selection and use of dropsonde-equipped aircraft for operational forecasting applications. *Bull. Amer. Meteor. Soc.*, 71, 1746-1756.

Forsythe, G. E., 1945: A generalization of the thermal wind equation to arbitrary horizontal flow. *Bull. Amer. Meteor. Soc.,* 26, 371-375.

Holton, J. R., 1992: *An Introduction to Dynamic Meteorology.* 3d. ed. Academic Press, 511 pp.

Hoshkins, B. J., 1990: Theory of extratropical cyclones. *Extratropical Cyclones: The Erik Palmén Memorial Volume,* C. W. Newton and E. O. Holopainen, Eds., Amer. Meteor. Soc., 64-80.

Kidder, S. Q., and T. H. Vonder Haar, 1995: *Satellite Meteorology: An Introduction.* Academic Press, 466 pp.

Koch, S. E., 2001: Real-time detection of split fronts using mesoscale models and WSR-88D radar products. *Wea. Forecasting,* 16, 35-55.

McMurdie, L., and C. Mass, 2004: Major numerical forecast failures over the Northeast Pacific. *Wea. Forecasting,* 19, 338-356.

Neiman, P. J., and M. A. Shapiro, 1989: Retrieving horizontal temperature gradients and advections from single-station wind profiler observations. *Wea. Forecasting,* 4, 222-233.

Parish, T. R., 1982: Barrier winds along the Sierra Nevada Mountains. *J. Appl. Meteor.*, 21, 925-930.

Parsons, K. E., and P. E. Smith, 2004: An investigation of extratropical cyclone development using a scale-separation technique. *Mon. Wea. Rev.,* 132, 956-974.

Petterssen, S., 1956: *Motion and Motion Systems.* Vol. 1, *Weather Analysis and Forecasting,* McGraw-Hill, 428 pp.

Reed, R. J., 1990: Advances in knowledge and understanding of extratropical cyclones. E*xtratropical Cyclones: The Erik Palmén Memorial Volume,* C. W. Newton and E. O. Holopainen, Eds., Amer. Meteor. Soc., 27- 45.

Truitt, J. B., 1994: West-coast analysis of approaching oceanic storms using thermal wind: a favorable coincidence for WSR-88D use. Postprints, *First WSR-88D Users Conf.,* Norman, OK, 74-82. [Available from NOAA/WSR-88D Operational Support Facility, 1313 Halley Circle, Norman, OK 73069.]

Uccellini, L. W., 1990: Processes contributing to the rapid development of extratropical cyclones. *Extratropical Cyclones: The Erik Palmén Memorial Volume,* C. W. Newton and E. O. Holopainen, Eds., Amer. Meteor. Soc., 81-105.

Young, M. V., and J. R. Grant, 1995: Interpreting features associated with baroclinic troughs. *Images in Weather Forecasting,* M. J. Bader, G. S. Forbes, J. R. Grant, R. B. E. Lilley, and A. J. Waters, Eds., Cambridge University Press, 287-301.

Acknowledgments

The author wishes to thank the two reviewers for the National Weather Digest for their constructive and highly detailed comments about the manuscript. They provided numerous needed recommendations. They are Dr. Jerome Patoux, Professor of Meteorology at the University of Washington, Seattle, and Dr. Scott Rochette, Associate Professor of Meteorology at the State University of New York (SUNY) at Brockport.

Dr. David Schultz, National Severe Storms Laboratory, provided both encouragement and an extra iteration during a prior review process that helped tighten the science and the text. Conversations with John Weaver, Research Meteorologist at NOAA, and Dan Bikos, Research Coordinator for the Cooperative Institute for Research in the Atmosphere, helped the cyclogenesis presentation. Tom Ainsworth, Meteorologist In Charge at WFO Juneau, provided suggestions to help readability as well as operational application. Gary Hufford, NWS Alaska Regional Scientist, and Audrey Rubel, Physical Scientist, provided a joint manuscript review and several of their recommendations have been applied.

Sarah Olsen served as computer graphics illustrator. Axel Graumann, meteorologist and Head of the Satellite Services Group within the National Climatic Data Center, provided the GOES IR image. Paul Shannon, then Lead Forecaster and currently the Information Technology Officer in Juneau, wrote the WSR-88D VWP script. Carl Dierking, Science and Operations Officer in Juneau, wrote the application used to log forecaster notes within the AWIPS environment, and provided a detailed review with several changes that have been applied.

Gary Ellrod, Chief Editor of National Weather Digest, encouraged elaboration on the possible satellite application of the method. He and Kermit Keeter, Technical Editor of National Weather Digest, provided finishing reviews that added to the text's clarity.